Mid-height Seismic Isolation of Equipment in Nuclear Power Plants

Kaivalya M. Lal[a*], Andrew S. Whittaker[b], Michael C. Constantinou[c]

[a] PhD Candidate, University at Buffalo, The State University of New York, Amherst, NY 14260
[b] SUNY Distinguished Professor, University at Buffalo, The State University of New York, Amherst, NY 14260
[*] Corresponding author: klal@buffalo.edu

Abstract

This paper introduces an innovative seismic isolation solution for designers of safety-class equipment in advanced nuclear power plants. The test specimen was a tall, slender, carbon steel vessel that could represent a reactor vessel, steam generator, or a heat exchanger: 240 inches tall, outer diameter of 60 inches, and wall thickness of 1 inch. The vessel was supported by three radial mounts at its mid-height, near its center of gravity, on a steel frame. The vessel was subjected to three component ground motions using an earthquake simulator at the University at Buffalo. The model was filled with water during testing to indirectly account for the fluid and internal equipment present inside a prototype vessel. Three configurations were tested: non-isolated, isolated using single Friction Pendulum (SFP) bearings, and isolated using triple Friction Pendulum (TFP) bearings. The test results demonstrate that mid-height seismic isolation is practical and enables a significant reduction in horizontal spectral accelerations. These outcomes are not specific to the spherical sliding bearings used in the experiments but are broadly applicable to mid-height, seismically isolated equipment.

Keywords: equipment isolation; mid-height seismic isolation; safety-class equipment; nuclear power plants; earthquake-simulator experiments

1. Introduction

Seismic isolation has been applied to more than 10,000 structures worldwide including hospitals, data centers, buildings of cultural importance, bridges, emergency operations facilities, offshore oil and gas platforms, port facilities, container cranes, and electrical substations and power distribution systems.

The benefits of seismically base isolating nuclear power plants (NPPs), in terms of reduced seismic demands and risk, are well established (e.g., Tajirian (1992), Tajirian and Patel (1993), Aiken *et al.* (2002), Huang *et al.* (2008; 2009), Kumar *et al.* [6; 7], Yu *et al.* (2018), but the technology is yet to be applied to an NPP (or a nuclear facility) in the United States. Parenthetically, seismic isolation is being considered as an integral design feature in some US advanced nuclear reactors, with the twin goals of steep reductions in capital cost and standardization of reactor designs [9; 10]. Outside the U.S., two NPPs, in Cruas, France and Koeberg, South Africa, were base isolated in the early 1980s to enable the re-use of a certified plant design developed for a site of lower seismic hazard. Seismic isolation has also been implemented in the International Thermonuclear Experimental Reactor (ITER), the Jules Horowitz Reactor (JHR), the La Hague spent fuel storage pool, and the Georges Besse II uranium enrichment facility, all in France, with ITER and JHR under construction at the time of this writing. In Japan, electric utilities have seismically isolated emergency operations buildings at the sites of NPPs (e.g., Kashiwazaki-Kariwa, Fukushima Daiichi, Fukushima Daini, and Onagawa) with the objective of ensuring the availability of emergency equipment and the safety of control-room staff after an earthquake. The isolated buildings at Fukushima Daiichi, Fukushima Daini, and Onagawa experienced significant shaking during the 2011 East Japan Earthquake and performed well, with no substantial damage reported [11].

The traditional implementation of seismic isolation involves installation of horizontally flexible and vertically stiff bearings (or isolators) at the base of a building. An alternate implementation, that could be considered where base isolation is impractical (e.g., a deeply embedded advanced reactor building), is to isolate safety-class equipment at their supports inside a nuclear facility. The concept of equipment isolation is not new. Traditionally known as vibration isolation, wherein a piece of equipment is placed atop elements (e.g., rubber bearings or spring-damper devices) that help reduce its response to an induced excitation, it has been studied for nearly 100 years. Seismic isolation is a specific application of vibration isolation. Kircher *et al.* (1979) studied the response of and designed an isolation system for a 230 kV circuit breaker using elastomeric bearings for the California Department of Water Resources. Kelly (1983) conducted shake table tests to demonstrate the benefits of seismically isolating nuclear power plant components using rubber bearings. In 1987, the Mark II Detector and Liquid Argon Calorimeter was isolated at the Stanford Linear

Accelerator Center using lead rubber bearings [14]. Kelly and Mayes (1989) proposed seismic isolation of fluid containing tanks supported on a large concrete basemat. Kelly and Mayes (1989), Tajirian (1993) and Zayas and Low (1995) analyzed the response of Liquified Natural Gas (LNG) tanks isolated using rubber bearings and Friction Pendulum bearings, respectively, and concluded that base isolation would significantly reduce demands in the tanks. Ersoy *et al.* (2001), Murota *et al.* (2005), and Oikonomou *et al.* [20; 21] conducted earthquake-simulator tests of power transformer models isolated using rubber and spherical sliding bearings. The successful outcomes of the Oikonomou *et al.* study led Bonneville Power Administration to isolate an existing high voltage transformer in 2013 and Seattle City Light to isolate a new high voltage power transformer in 2014 [22]. Others have studied seismic isolation of equipment, all of which, including those mentioned above, have focused on base isolating equipment, which may not be a practical solution for tall, slender equipment due to large base overturning moments during earthquake shaking, resulting in substantial tensile axial forces or possible uplift in the bearings.

This paper focuses on mid-height seismic isolation of equipment: an innovative application not studied previously and considered here to expand the range of options available to designers of safety-class equipment in advanced reactors. The following sections describe earthquake-simulator experiments of a half-length scale tall, slender vessel that could represent a reactor vessel, a steam generator, or a heat exchanger in an advanced nuclear power plant (e.g., Figures 3 and 4 in Parsi *et al.* (2022). The vessel was seismically isolated using spherical sliding bearings. The goals of the experiments were to 1) demonstrate the utility and benefits of mid-height seismic isolation, and 2) build a dataset to support validation of numerical models.

2. Test specimen

2.1. Vessel and support frame

The test specimen was a cylindrical, carbon steel (ASTM A36) vessel with an outer diameter of 60 inches, a height of 240 inches, and a wall thickness of 1 inch. The length scale of 0.5 is based on the physical sizes of a proposed high temperature gas reactor and a proposed steam generator. The vessel was fabricated in two pieces, one 150 inches tall and the other 90 inches tall. The lower 150-inch tall section had a 1-inch thick end plate welded at its bottom and a 1-inch thick flange welded at its top. The upper 90-inch tall section was a cylinder with 1-inch thick flanges welded at both its ends. Twenty-four equally spaced holes were drilled in the flanges to enable a bolted connection between the two sections of the vessel. A 1/8-inch thick EPDM rubber gasket was installed between the two sections to prevent loss of water. The vessel was supported at its mid-height on a stiff steel frame by three equally spaced mounts. The mounts were welded to the vessel wall and connected to each other via shaped plates to achieve diaphragm action at the isolation plane. The vessel was filled with water to indirectly account for the fluid and internal equipment inside a prototype vessel.

The steel frame had plan dimensions of 116 in $\times$ 116 in and was 121 inches tall. The frame had four W10 $\times$ 22 corner columns concentrically braced with $6 \times 6 \times 1$ angles to provide lateral stiffness, and three W8 $\times$ 58 interior columns, one beneath each support mount, to provide vertical support to the vessel. The corner columns were joined by 6-inch deep by 1-inch thick plates, welded to a 1-inch thick mounting plate with a central 76-inch diameter hole. The steel frame was bolted directly to the earthquake simulator. Figure 1 shows the test assembly installed on the earthquake simulator. A rectangular plate, identified as Vessel head in Figure 1, was bolted to the top flange of the 90-inch tall upper section to attach sample internals (see Section 2.2). To prevent loss of water during testing, a 1/8-inch thick EPDM rubber gasket was installed between the rectangular plate and the vessel flange. The weight of the vessel including water, head, and internals was 39.3 kips. The total weight of the specimen and the steel frame was 49.3 kips. (The weight of the empty vessel, including the head and the internals, was 16.3 kips. The weight of the support frame was 10 kips. The weight of water inside the vessel was 23 kips.)

Three configurations of the specimen were tested: 1) non-isolated, wherein load cells were installed atop the steel frame and the vessel was bolted to the load cells via the three support mounts, 2) isolated using three single Friction Pendulum bearings (described in Section 2.3), wherein bearings were installed above the load cells and beneath the support mounts of the vessel, and 3) isolated using three Triple Friction Pendulum bearings (described in Section 2.3), wherein bearings were installed between the load cells and the support mounts. Figure 2 presents photographs of the installed bearings. (The bearings used in the experiments did not include a perimeter strip of cover rubber, which is used for field applications to prevent the ingress of moisture, dust, and debris. The perimeter strip of cover rubber

offers no significant lateral resistance and is torn upon significant movement of a bearing, requiring replacement after significant earthquake shaking.)

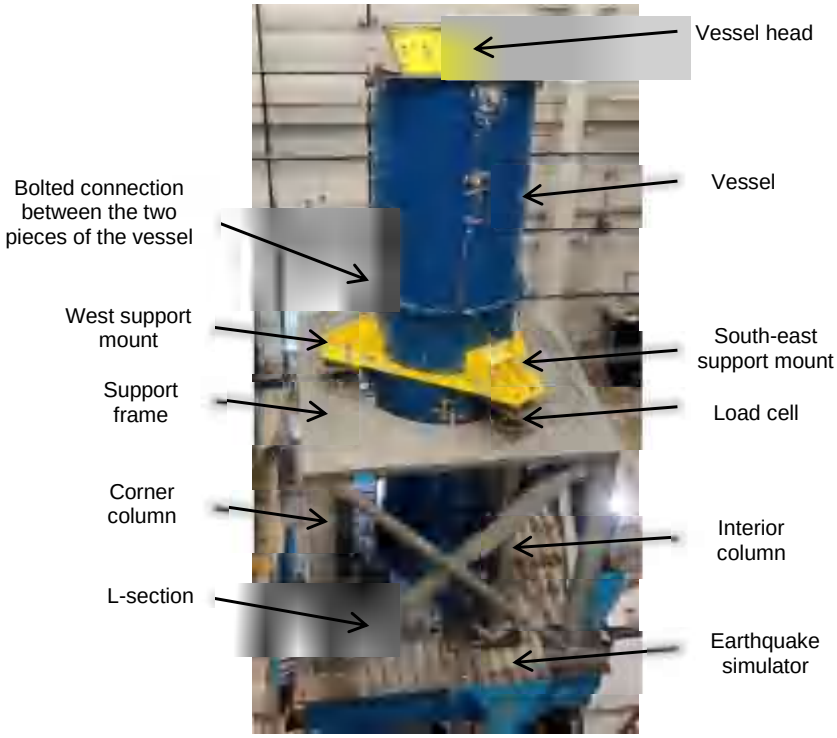

Figure 1. Test assembly on the earthquake simulator

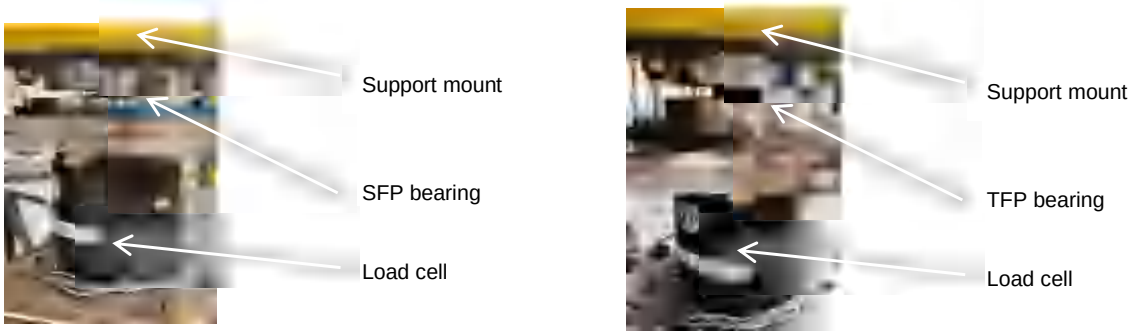

a) SFP bearing b) TFP bearing

Figure 2. Installed bearings in the isolated configurations of the vessel

2.2. Internals

Two internals were attached to the vessel head: 1) a 6-ft long aluminum tube with a 3-inch outer diameter, a wall thickness of 0.125 in, and first mode frequency of about 7 Hz in air [23], and 2) a 6-ft long rectangular carbon steel plate with plan dimensions of 0.5 in × 6 in and a first mode frequency of about 3 Hz in air [23]. Figure 3 is a photograph of the internals attached to the vessel head.

2.3. Isolation systems

Two types of spherical sliding bearings were used for the mid-height isolation of the test vessel: single concave Friction Pendulum (SFP) bearings and triple Friction Pendulum (TFP) bearings. The SFP bearings consist of an articulated slider coated with a PTFE-type composite, a sliding surface of polished stainless steel, and a housing plate. Figure 4 presents the cross section and internal construction of the SFP bearings. The SFP bearings had a sliding period of 1.38 seconds (frequency of 0.72 Hz) and a displacement capacity of 3.5 inches.

The TFP bearings consist of two concave plates and a nested slider assembly. The nested slider assembly, which is surrounded by a perimeter rubber seal, consists of two concave slide plates separated by a rigid slider. The surfaces of the slide plates in contact with the outer concave plates and the two surfaces of the rigid slider are coated with a PTFE-type material. Sliding is permitted on all four polished stainless steel concave surfaces. Figure 5 presents the cross section and internal construction of the TFP bearings. The concave surfaces in a TFP bearing are numbered 1 through 4 in Figure 5a. The TFP bearings had a sliding period (for sliding on outer concave surfaces) of 1.96 seconds (frequency of 0.51 Hz) and a displacement capacity of approximately 6.5 inches.

To determine the coefficients of friction on the sliding surfaces, the Friction Pendulum bearings were tested under combined axial and unidirectional shear loads in a test machine at the University at Buffalo. The axial and horizontal loads on the bearing and the sliding velocity in the characterization tests were similar to those expected in the earthquake simulator tests. The coefficients of friction were determined using procedures outlined in Constantinou *et al.* (2007) and values are reported Table 1.

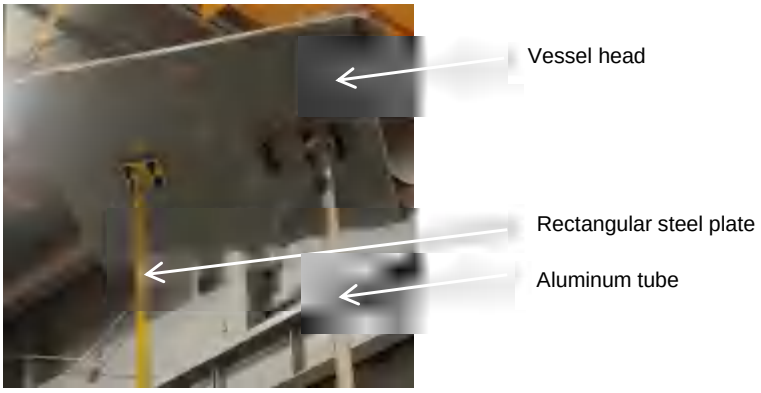

Figure 3. Installed internals

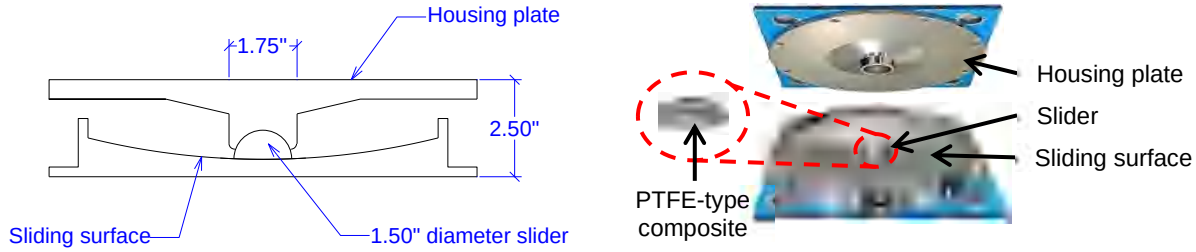

a) cross section b) internal construction

Figure 4. SFP bearing

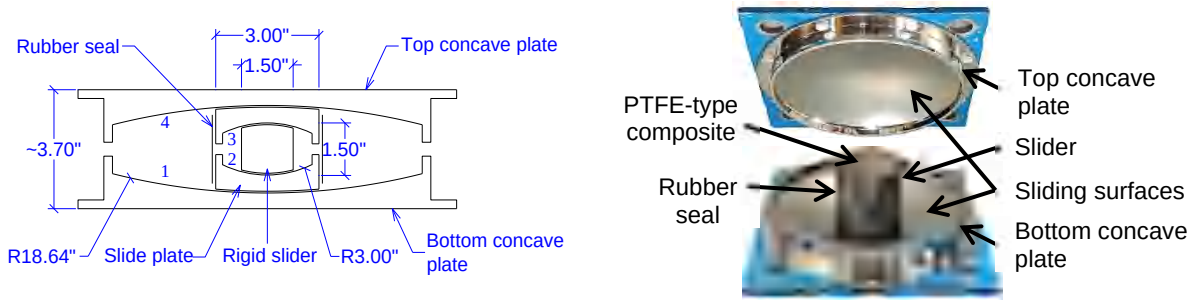

a) cross section b) internal construction

Figure 5. TFP bearing

3. Instrumentation and data acquisition

The response of the test specimen was recorded using time series of accelerations, hydrodynamic pressures, and horizonal displacements at different elevations on the vessel, forces and displacements in the bearings, and strains and accelerations on the internals. Figure 6 locates the instruments on the vessel and some key dimensions. Accelerometers were placed at the top and bottom of the vessel, and at its mid-height on the support mounts. String potentiometers measured horizontal displacements at the top, bottom, and mid-height of the vessel with respect to a reference frame on the ground. Hydrodynamic pressures on the vessel wall were measured using pressure gages, placed in arrays of four at three elevations. Two internals, shaded in green in Figure 6, were mounted on the vessel head. For each internal, waterproofed accelerometers were installed at their mid-height and tips. Strains near the points of attachment of the internals were measured using waterproofed strain gages.

Figure 7 presents the location of instruments on the earthquake-simulator and the support frame and some key dimensions. Accelerometers were installed on the earthquake simulator to record the seismic inputs. Accelerometers were also installed at the load cell-to-bearing interfaces to measure accelerations below the isolation system and atop the steel frame. The forces in the bearings were measured using calibrated five-channel load cells, placed beneath the bearings (see Figure 2). The displacements of the bearings were measured using string potentiometers. String potentiometers were also installed at the load cell-to-bearing interfaces to measure the displacements at that level with respect to the ground.

Table 1. Coefficients of friction (%) for SFP and TFP bearings

	SFP		TFP			
			$\mu_2 = \mu_3$		$\mu_1 = \mu_4$	
	μ_{slow}	μ_{fast}	*slow*[1]	*fast*[1]	*slow*[1]	*fast*[1]
Bearing 1	2.8	7.6	0.8	2.0	6.8	11.0
Bearing 2	2.7	7.6	0.5	1.5	6.3	11.5
Bearing 3	3.0	8.4	1.0	2.0	7.1	11.3

1. *Slow* and *fast* characterize the velocity of the slider

4. Seismic inputs

Ground motions were selected from PEER NGA-West 2 database to cover a broad range of frequencies: from approximately 0.2 Hz to 45 Hz in the two horizontal directions (H1 and H2) and 0.2 Hz to 70 Hz in the vertical direction (V). The frequency range of interest was determined based on modal analyses of a preliminary model of the test specimen in computer program SAP2000 [25]. Three ground motions were selected: 1) Record Sequence Number (RSN) 587, peak ground acceleration (PGA) H1 = 0.28 g, H2 = 0.24 g, V = 0.14 g, 2) RSN 728, PGA H1 = 0.17 g, H2 = 0.21 g, V = 0.23 g, and 3) RSN 796, PGA H1 = 0.10 g, H2 = 0.20 g, V = 0.06 g. The time scale of all three components of the ground motions was reduced by a factor of 0.71, consistent with the assumed length scale of 0.5. Figure 8 presents 5% damped acceleration response spectra of the time-scaled ground motions. Multisine excitation with a frequency range of 0.25 to 100 Hz and an amplitude of 0.1 g was imposed on the non-isolated test specimen prior to earthquake testing to identify its modal frequencies.

The ground motions were amplitude scaled to achieve different intensities of shaking. The maximum values of the scale factors were selected so as to not exceed: 1) the displacement, velocity, and acceleration capacities of the horizontal and vertical actuators of the earthquake simulator, 2) the displacement capacities of the SFP and TFP bearings, and 3) stress in the wall and support mounts of the vessel, in the non-isolated configuration, of 36 ksi (i.e., the yield strength of the ASTM A36 carbon steel) with a margin. A preliminary SAP2000 model of the test specimen was analyzed to estimate the bearing displacements and stresses in the wall and support mounts of the vessel.

Earthquake-simulator tests were performed using unidirectional (1D), bi-directional (2D), and tri-directional (3D) inputs. This paper presents results of the 3D tests. The test sequences for the non-isolated, SFP-isolated, and TFP-isolated configurations are presented in Table 2. Data from all the tests (1D, 2D, and 3D tests) are archived at DesignSafe.

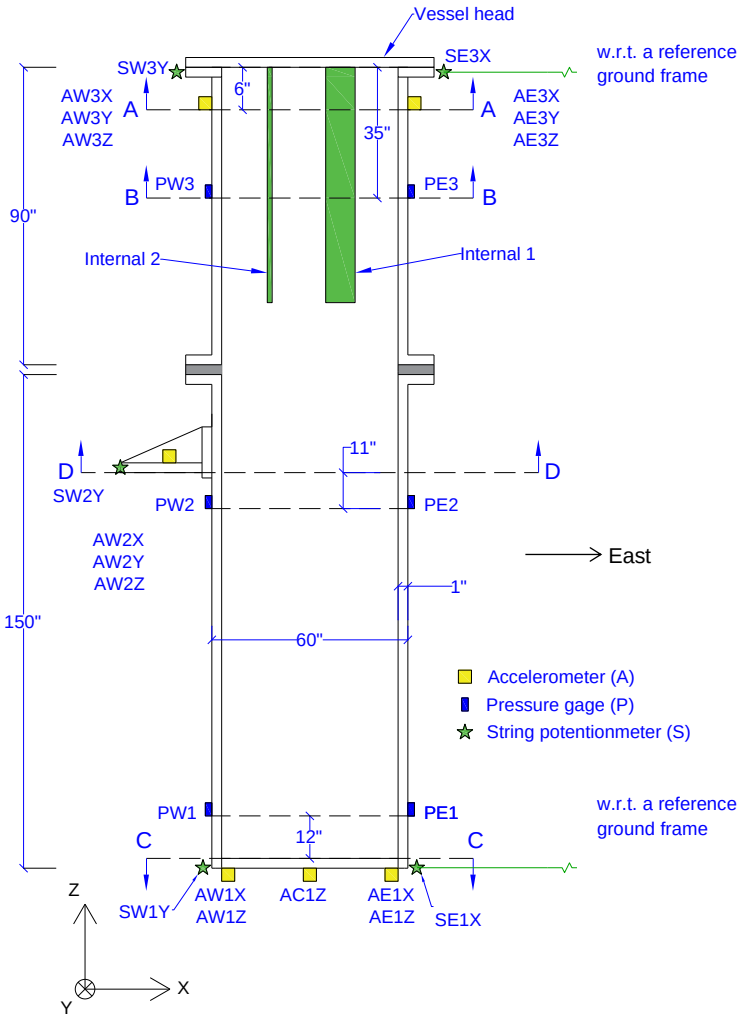

a) elevation

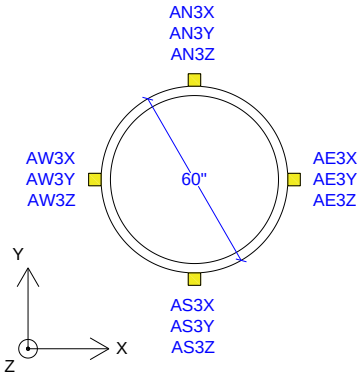

b) section A-A

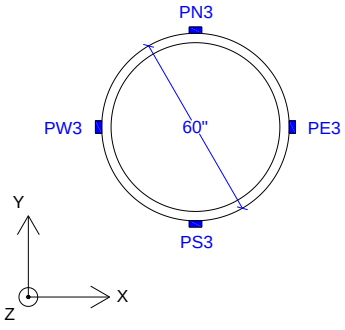

c) section B-B

Figure 6. Overall dimensions and instrumentation of the vessel

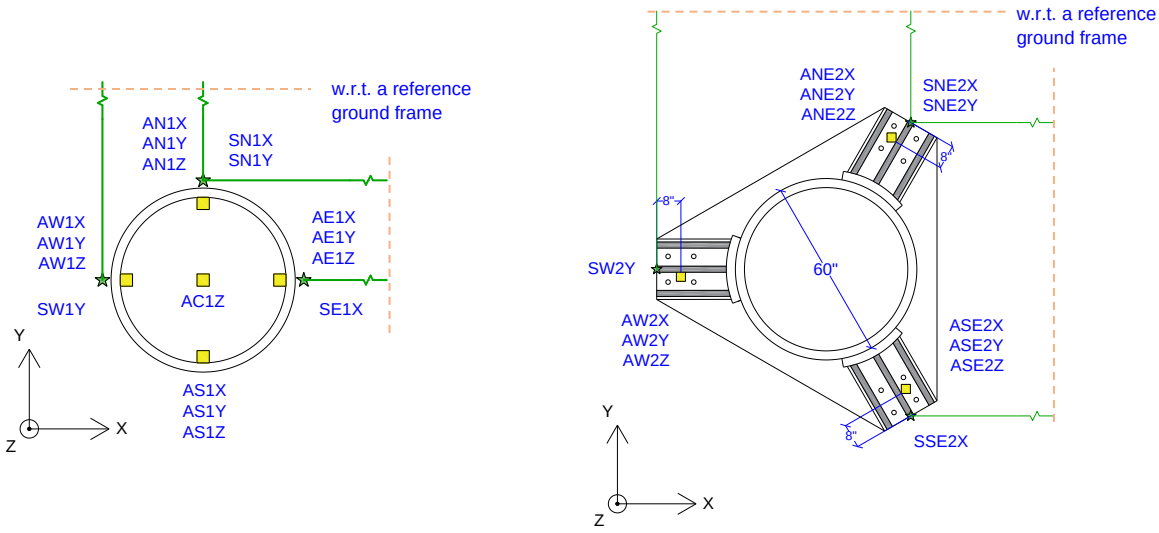

d) section C-C e) section D-D

Figure 6. Overall dimensions and instrumentation of the vessel (cont.)

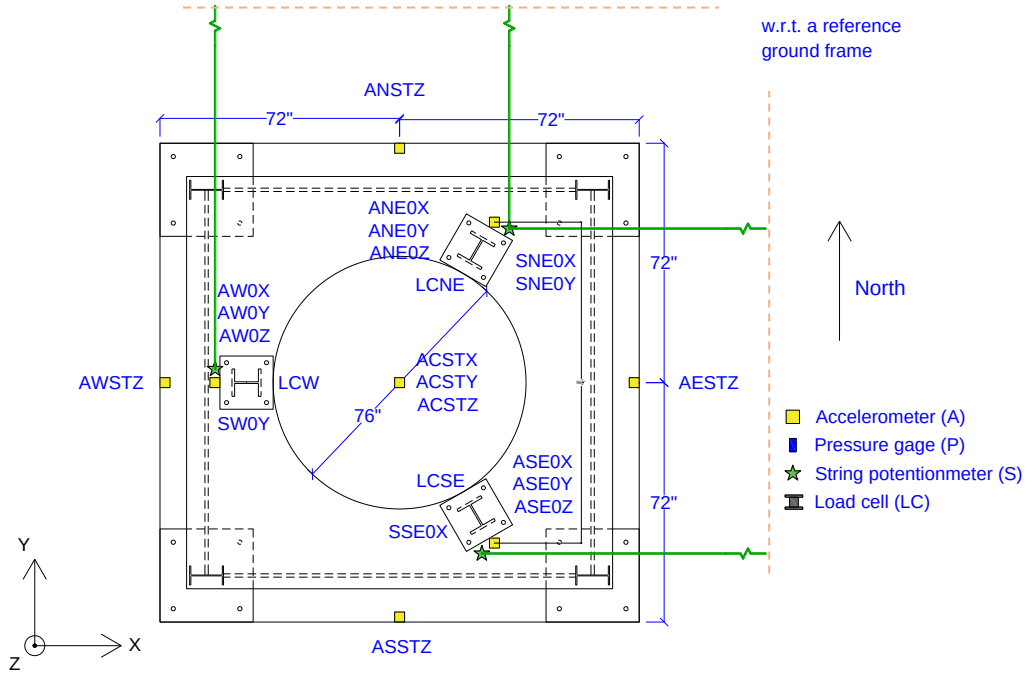

a) plan

Figure 7. Dimensions and instrumentation of the support frame and the earthquake simulator

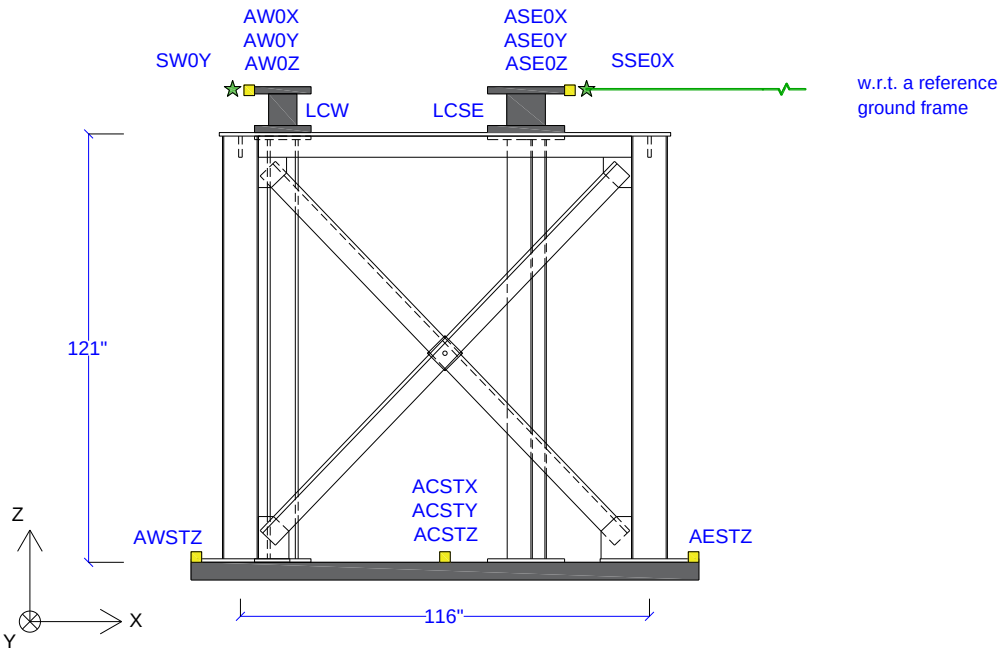

b) south elevation

Figure 7. Dimensions and instrumentation of the support frame and the earthquake simulator (cont.)

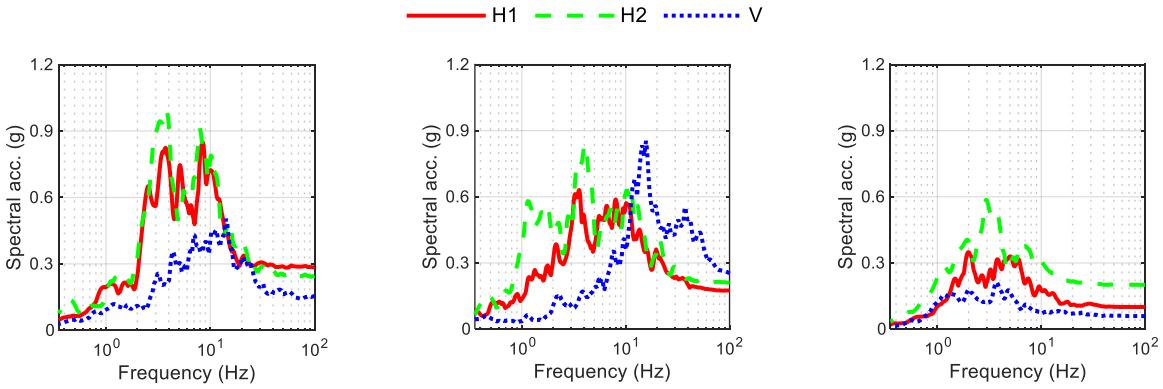

a) GM1 b) GM2 c) GM3

Figure 8. Acceleration response spectra of the time-scaled ground motions, 5% damping

Table 2. Testing sequence for the 3D tests

#	Test	Geomean horizontal PGA (g)[1]	Vertical PGA (g)
	Non-isolated vessel		
1	FB1A-3D	0.20	0.11
2	FB1B-3D	0.40	0.22
3	FB2A-3D	0.20	0.25
4	FB2B-3D	0.35	0.43
5	FB3A-3D	0.10	0.04
6	FB3B-3D	0.25	0.10
	SFP-isolated vessel		
1	SF1A-3D	0.20	0.11
2	SF1B-3D	0.60	0.33
3	SF2A-3D	0.20	0.25
4	SF2B-3D	0.35	0.43
5	SF3A-3D	0.10	0.04
6	SF3B-3D	0.25	0.10
	TFP-isolated vessel		
1	TF1A-3D	0.20	0.11
2	TF1B-3D	0.60	0.33
3	TF2A-3D	0.20	0.25
4	TF2B-3D	0.50	0.61
5	TF3A-3D	0.10	0.04
6	TF3B-3D	0.30	0.12

1. $\sqrt{\text{PGA of horizontal component 1} \times \text{PGA of horizontal component 2}}$

5. Test results

5.1. Introduction

The amplitudes of the seismic inputs and simulator-specimen interaction[1] were different for the non-isolated and isolated configurations. Accordingly, only a qualitative comparison of specimen responses in the non-isolated and isolated configurations is presented to demonstrate the feasibility and benefits of mid-height seismic isolation. The

[1] Simulator-specimen interaction was observed due to the large relative weight of the specimen (= 49.3 kips versus the simulator platform weight of 24 kips), the high center-of-mass of the specimen with respect to the earthquake-simulator platform, and cross talk between the simulator's vertical and horizontal actuators. Due to simulator-specimen interaction, the accelerations recorded at the center of earthquake simulator were slightly higher than the target seismic inputs of Table 2.

solid pink circles in Figure 9 identify locations on the test specimen and the earthquake simulator where results are reported.

The test results presented in this paper include:

1) Horizontal and vertical acceleration response spectra and peak accelerations:
   a) At the center of the earthquake-simulator platform (location *C1* in Figure 9).
   b) Atop the load cell on the north-east side (location *F1*). It represents the acceleration response at the mid-height of the vessel, at the level of support mounts, for the non-isolated configuration, and directly below the isolation plane for the isolated configurations. (North is defined in Figure 9.)
   c) On the north-east support mount of the vessel for the isolated configurations (location *V1*), representing the acceleration response directly above the isolation plane.
   d) At the top and the bottom of the vessel on the north face (locations *V2* and *V3*).
2) Rocking acceleration spectra about the two horizontal axes:
   a) At the center of the earthquake-simulator. (There were no rocking inputs to the earthquake simulator, but rocking resulted from simulator-specimen interaction and compliance between the simulator's horizontal and vertical actuators.)
   b) At the top and the bottom of the vessel.
3) Peak accelerations at the bottom of internal 1 (location *N1*).
4) Peak axial strains in the submerged internals (locations *N2* and *N3*).
5) Normalized force-displacement loops for the isolation systems.

Identical acceleration histories were recorded in each direction on a) the north-east, south-east, and west load cells, b) the north-east, south-east, and west support mounts and c) the north, east, west, and south faces of the vessel at its top and bottom. Rocking acceleration histories about the *x*- and *y*-axes were determined by calculating the difference in vertical (*z*) acceleration responses and dividing by the distance between the accelerometers.

The force-displacement loops for the isolation systems were derived by normalizing the total instantaneous horizontal force in each direction by the total instantaneous normal load on the bearings. The total horizontal (normal) force is the sum of the shear (axial) forces in the load cells mounted beneath the bearings. Displacement histories were recorded at the top of the load cells, just below the isolators, and at the level of the supporting mounts of the vessel, just above the isolators. Isolator displacements were calculated as the difference between the displacement histories above and below the bearings. Displacement was measured at two locations in each direction: for the north-east and south-east bearings in the *x* direction, and the north-east and west bearings in the *y* direction, as identified in Figure 6e. The isolated vessel did not rotate about its longitudinal axis, as established by comparing the isolator displacement histories from the two sets of recordings in each direction. The *x*- and *y*-direction isolator displacement histories for the north-east bearing were used to generate the normalized force-displacement loops.

5.2. System identification

The modal frequencies of the test specimen were derived using frequency response functions (FRFs) from multisine tests of the non-isolated configuration. The FRFs were generated using acceleration histories measured at the top and bottom of the vessel and at the center of the earthquake simulator. The modal frequencies in the vertical direction were 17 Hz and 45 Hz. The interior columns, load cells, bearings, and vessel support mounts contribute to the vertical flexibility of the specimen. The peaks in the FRFs in the *x*- and *y*-directions were at 11 Hz and correspond to the rocking of the vessel, as confirmed by the peaks observed at 11 Hz in the rotational FRFs. No horizontal mode frequencies of the support frame and of the vessel were computed because their horizontal stiffness was very high.

5.3. Non-isolated configuration

Figure 10 presents 5% damped acceleration response spectra for test FB1B-3D in Table 2 at the locations identified in Section 5.1. Results for the other five tests are presented in a Digital Appendix [26]. Table 3 presents the peak accelerations, calculated here as spectral acceleration at 100 Hz, for the six 3D tests. Accelerations from the center of

the earthquake simulator[2] were amplified by the support frame to the support mounts of the vessel, from location *C1* to *V1*[3]: compare the green dashed and black solid lines in panels a through c of Figure 10. Identical trends were observed for the other tests. The peak horizontal (vertical) accelerations were amplified by the support frame by a factor of between 1.4 (1.2) and 1.8 (2.9). Significant variation was expected because of differences in the frequency content of the input motions.

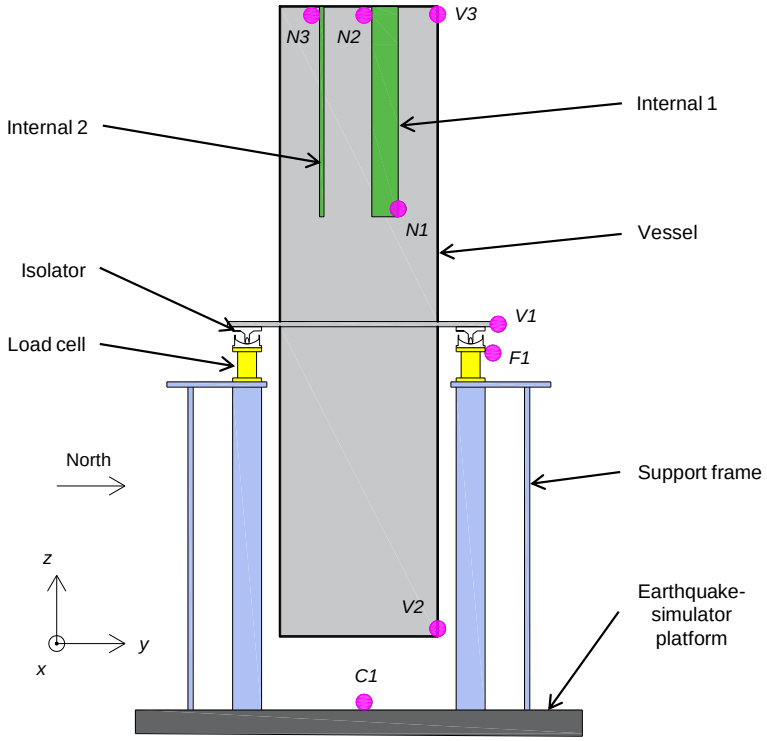

Figure 9. Monitoring locations (solid pink circles) for presenting earthquake-simulator test results

Accelerations at top of the load cells (location *V1*) were amplified to the top and the bottom of the vessel (locations *V2* and *V3*), with an increase in peak values by a factor of between 1.2 (1.6) and 2.2 (1.9) in the horizontal (vertical) direction[3]. The vertical response of the vessel was driven by its vertical modes at 17 Hz and 45 Hz, and its horizontal response by rocking at 11 Hz. The rocking of the vessel was amplified by the rocking of the earthquake-simulator platform due to simulator-specimen interaction.

At the bottom of internal 1, the peak accelerations were amplified by a factor of between 1.9 (1.1) and 2.4 (1.4) in the horizontal (vertical) direction with respect to the top of the vessel (from location *V3* to *N1*). Table 4 presents peak axial strains in the two internals, measured near their points of attachments to the vessel head, at locations *N2* and *N3*, where maximum strains (and corresponding stresses) were expected. The peak strains in both the internals were between 5% and 22% of the corresponding yield strain. (Internal 1 was constructed of aluminum, and internal 2 from carbon steel. The specified minimum yield stress and the elastic modulus for the aluminum internal were 40 ksi and 10,000 ksi, respectively, with a corresponding yield strain of 4000 μS. The specified minimum yield stress and the elastic modulus for the carbon steel internal were 36 ksi and 29,000 ksi, respectively, with a yield strain of 1240 μS.)

[2] Accelerations at the center of the earthquake-simulator platform were used instead of those of the input motions of Section 4 due to specimen-structure interaction (see footnote 1).

[3] The vessel was bolted directly to the load cells in the non-isolated configuration, for which the acceleration histories at locations *V1* and *F1* in Figure 9 were identical.

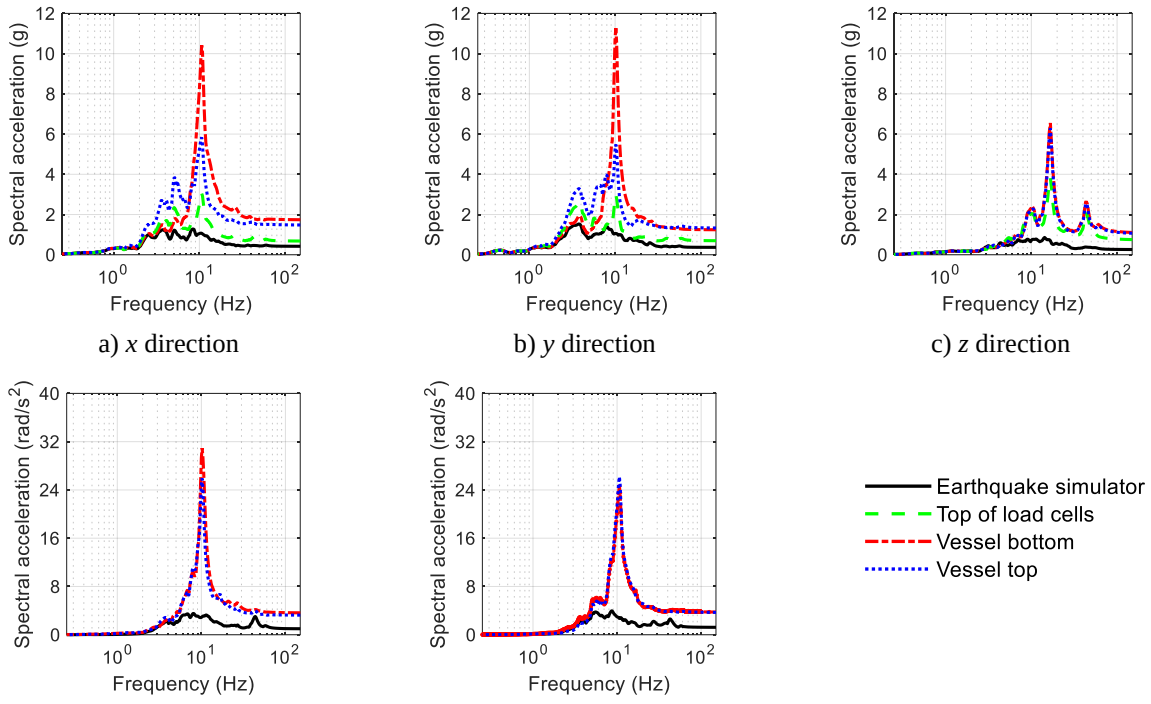

a) *x* direction b) *y* direction c) *z* direction

d) rocking about *x* axis e) rocking about *y* axis

Figure 10. Acceleration response spectra, test FB1B-3D, 5% damping

5.4. Isolated configurations

5.4.1. SFP-isolated

Results from the test SF1B-3D are presented herein. Companion results for the other tests are presented in the Digital Appendix [26]. Figure 11 presents 5% damped acceleration response spectra directly above and below the isolation plane (locations *V1* and *F1*). The vertical thin blue lines in these figures at a frequency of 0.72 Hz correspond to the sliding period (1.38 seconds) of the SFP bearings. Table 5 presents the peak accelerations at locations identified in Section 5.1 for the six 3D tests. The support frame amplified the motions at the center of the earthquake simulator (location *C1*) to the underside of the isolation plane (location *F1*) for frequencies greater than 10 Hz (compare the black solid and red dashed lines in Figure 11), with increases in peak accelerations by a factor of between 1.1 (1.0) and 1.6 (1.5) in the horizontal (vertical) direction. For frequencies greater than 3 Hz (of interest for the vessel and its internals herein), the horizontal spectral accelerations above the isolation plane were generally substantially smaller than those below the isolation plane: compare the green and red dashed lines in panels a and b of Figure 11. Identical trends were observed for the other tests of the SFP-isolated vessel. The peak horizontal accelerations above the isolation plane were reduced by a factor of between 1.5 and 3.4 with respect to those below the isolation plane.

Figure 12 presents normalized horizontal force-displacement loop for the SFP isolation system. The fluctuation in the coefficient of friction in the normalized loops was due to a) its dependance on the sliding velocity, b) its dependance on the contact pressure on the slider (see Constantinou *et al.* (2007)), and c) rotation of the concave plates of the bearings, attached to the support mounts of the vessel (see Fenz and Constantinou (2008)).

Figure 13 presents acceleration response spectra at the top and the bottom of the vessel (locations *V2* and *V3*). For frequencies greater than 3 Hz, the amplitude of the horizontal spectral acceleration was significantly smaller than those in the non-isolated configurations. For example, compare the red dashed lines (spectra at the top of the vessel) in panels a and b of Figures 10 and 13. Trends for the other tests were identical. Depending on the amplitude and frequency content of the input motion, the peak horizontal accelerations at the top and the bottom of the vessel were reduced by a factor of between 1.1 and 2.5 with respect to those below the isolation plane. For the smaller amplitude motions, wherein the SFP bearings operated primarily in the elastic range, the benefit of isolation was small. The

Table 3. Peak accelerations[1] (g) for the 3D tests of the non-isolated configuration, *x*, *y*, and *z* directions[2]

Test	Earthquake simulator			Atop load cells			Vessel bottom			Vessel top			Internal 1 bottom		
	x	***y***	***z***	***x***	***y***	***z***	***x***	***y***	***z***	***x***	***y***	***z***	***x***	***y***	***z***
FB1A-3D	0.23	0.18	0.12	0.34	0.33	0.32	0.72	0.65	0.46	0.67	0.66	0.44	2.20	0.93	0.53
FB1B-3D	0.42	0.37	0.26	0.68	0.69	0.73	1.73	1.24	1.07	1.47	1.32	1.04	3.73	1.83	1.25
FB2A-3D	0.24	0.29	0.20	0.39	0.35	0.57	0.96	0.47	0.86	0.55	0.50	0.83	1.47	0.89	1.05
FB2B-3D	0.42	0.54	0.34	0.72	0.63	0.98	1.69	0.85	1.44	0.98	0.93	1.39	2.55	1.46	1.88
FB3A-3D	0.08	0.15	0.05	0.16	0.20	0.06	0.16	0.26	0.08	0.22	0.34	0.08	0.58	0.49	0.08
FB3B-3D	0.19	0.39	0.12	0.38	0.51	0.18	0.45	0.63	0.23	0.56	0.85	0.22	1.51	1.27	0.26

1. Peak acceleration calculated as spectral acceleration at 100 Hz
2. See Figure 6 for the global co-ordinate system

Table 4. Peak axial strains (μS) in internals for the 3D tests of the non-isolated configuration[1]

Test	Internal 1	Internal 2
FB1A-3D	427	140
FB1B-3D	749	231
FB2A-3D	373	185
FB2B-3D	569	268
FB3A-3D	206	123
FB3B-3D	486	235

1. For reference, the yield strain in internal 1 (internal 2) is approximately 4000 (1240) μS

response of the vessel in the vertical direction was driven by the vertical modes of the frame-bearing-vessel system with modal frequencies at 14 Hz and 38 Hz. The peak vertical accelerations were 1.1 to 2.2 times greater than those at the underside of the isolation plane. The vertical flexibility of the isolators resulted in the frequency shift to 14 Hz (38 Hz) from 17 Hz (45 Hz) in the non-isolated configuration.

The isolated vessel rocked at a frequency of approximately 8 Hz (see Figure 13d and 13e): lower than the non-isolated rocking frequency of 11 Hz. Although vessel rocking amplified its horizontal response near 8 Hz (see the green arrow in Figure 13a), the rotational response of the SFP-isolated vessel was substantially smaller than the non-isolated vessel for similar rocking inputs to the earthquake-simulator: compare Figures 10d and 13d for which the rocking input at 100 Hz is approximately 0.9 rad/sec2 in both cases.

The peak accelerations at the bottom of internal 1 (location *N1*) were amplified by a factor of between 2.5 (1.2) and 3.4 (2.2) in the horizontal (vertical) directions with respect to the top of the vessel (location *V3*). Table 6 presents peak axial strains in the two internals, at locations *N2* and *N3*, with values of between 3% and 10% of the corresponding yield strains.

5.4.2. TFP-isolated

Results for the test TF1B-3D are presented here. The Digital Appendix [26] presents results for other 3D motions. Figure 14 presents 5% damped acceleration response spectra directly above and below the isolation plane (locations *V1* and *F1*). The vertical thin blue lines in these figures at a frequency of 0.51 Hz correspond to the sliding period (1.95 seconds) of the outer two surfaces of the TFP bearings. Peak accelerations for the six 3D tests are reported in Table 7. The amplification by the support frame (from location *C1* to *F1*) was similar to that in the SFP-isolated configuration. The spectral accelerations above the isolation plane, for frequencies greater than 3 Hz, were generally substantially smaller than those below the isolation plane, with reductions in peak accelerations by a factor of between 1.5 and 4.2. The percentage reduction was generally higher than in the SFP-isolated configuration because of the adaptive behavior of TFP bearings, that is, sliding on multiple concave surfaces [28]. For small amplitude shaking, sliding occurs on the inner surfaces where the coefficients of friction are less than those for the outer surfaces (see Table 1). Figure 15 presents normalized force-displacement loops for the TFP isolation system. The fluctuation in the coefficients of friction in the normalized loops is explained in Section 5.4.1.

Acceleration response spectra at the top and the bottom of the vessel (locations *V2* and *V3*) are presented in Figure 16. Like that in the SFP-isolated configuration, the amplitude of horizontal spectral accelerations for frequencies greater than 3 Hz were lower than those in the non-isolated configuration. The decreases in horizontal peak accelerations at the vessel top and bottom were by a factor of between 1.2 and 3.3 with respect to the underside of the isolation plane. The vertical and rocking responses of the TFP-isolated vessel were similar to those reported above for the SFP-isolated vessel.

At the bottom of internal 1 (location *N1*), the peak horizontal (vertical) accelerations were amplified by a factor of between 1.5 (1.2) and 2.9 (2.3) with respect to the top of vessel (location *V3*). Peak axial strains in the internals (at locations *N2* and *N3*), reported in Table 8, were between 2% and 12% of the corresponding yield strains.

6. Summary and conclusions

The earthquake-simulator experiments described in this paper were designed to assess the feasibility and demonstrate the benefits of mid-height seismic isolation of tall, slender equipment planned for some advanced reactors. A 240-inch tall vessel with an outer diameter of 60 inches and a wall thickness of 1-inch was utilized for the experiments. The test article was an approximate one-half length scale model of a proposed high temperature gas reactor and a steam generator. Two internals were attached to the vessel head as described in Section 2.2. Three configurations of the vessel were tested: 1) non-isolated, 2) SFP-isolated, and 3) TFP-isolated. The isolation bearings were characterized prior to earthquake-simulator testing. Ground motions with a broad range of frequency content and different amplitudes were used for the earthquake-simulator tests, consistent with the length scale factor of 0.5.

In the non-isolated configuration, the peak accelerations at the top of the load cells were amplified by a factor of between 1.2 (1.6) and 2.2 (1.9) to the top and the bottom of the vessel in the horizontal (vertical) directions. The

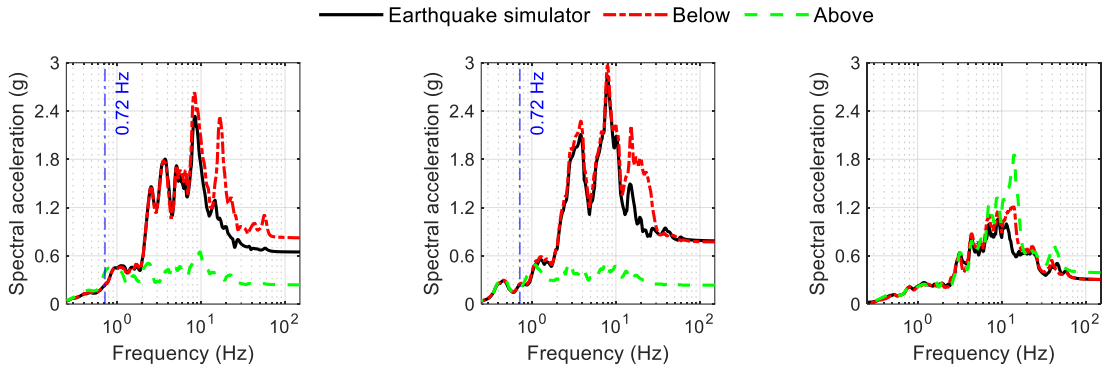

a) *x* direction b) *y* direction c) *z* direction

Figure 11. Acceleration response spectra directly above and below the isolation plane, test SF1B-3D, 5% damping

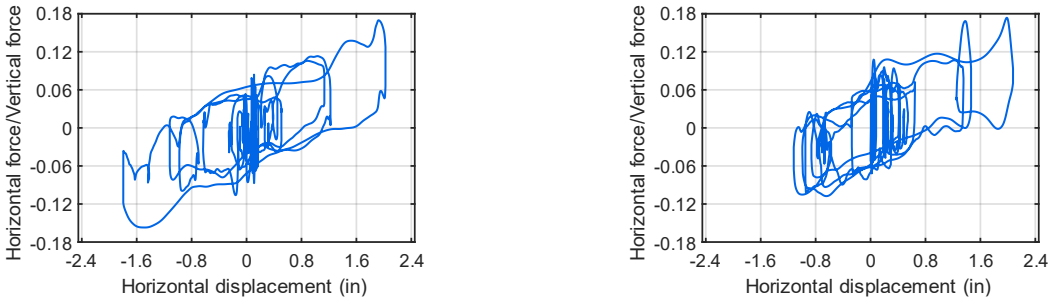

a) *x* direction b) *y* direction

Figure 12. Normalized force-displacement loops for the isolation system, test SF1B-3D

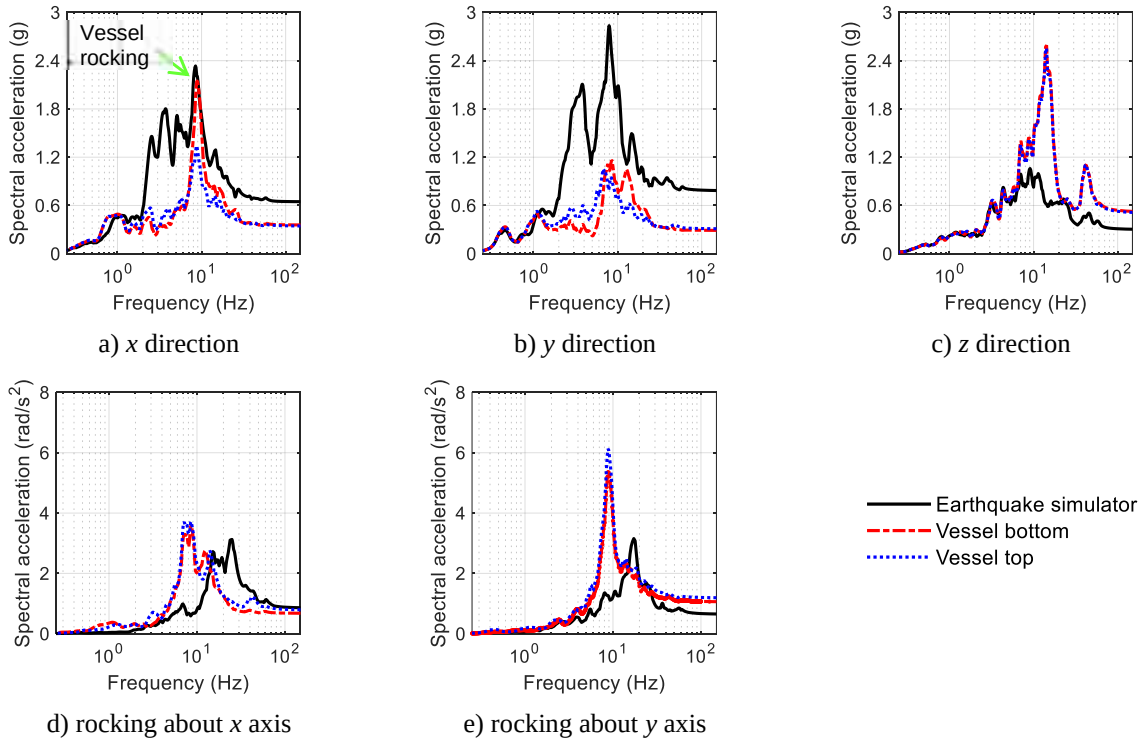

a) *x* direction b) *y* direction c) *z* direction

d) rocking about *x* axis e) rocking about *y* axis

Figure 13. Acceleration response spectra at the top and bottom of the vessel, test SF1B-3D, 5% damping

Table 5. Peak acceleration[1] (g) for the 3D tests of the SFP-isolated configuration, *x*, *y*, and *z* directions[2]

Test	Earthquake simulator			Directly above (below) the isolation plane			Vessel bottom			Vessel top			Internal 1 bottom		
	x	***y***	***z***	***x***	***y***	***z***	***x***	***y***	***z***	***x***	***y***	***z***	***x***	***y***	***z***
SF1A-3D	0.25	0.29	0.11	0.13 (0.30)	0.12 (0.30)	0.21 (0.16)	0.22	0.22	0.34	0.22	0.24	0.34	0.75	0.71	0.43
SF1B-3D	0.65	0.78	0.30	0.24 (0.82)	0.23 (0.77)	0.39 (0.30)	0.36	0.29	0.52	0.34	0.31	0.50	1.06	0.62	0.68
SF2A-3D	0.20	0.23	0.18	0.11 (0.24)	0.11 (0.26)	0.21 (0.20)	0.20	0.14	0.32	0.19	0.19	0.32	NR[3]	0.61	0.50
SF2B-3D	0.42	0.33	0.31	0.24 (0.69)	0.18 (0.48)	0.57 (0.38)	0.39	0.27	0.83	0.36	0.27	0.83	NR[3]	0.74	1.84
SF3A-3D	0.09	0.20	0.04	0.10 (0.16)	0.11 (0.25)	0.06 (0.05)	0.11	0.20	0.07	0.14	0.22	0.07	0.46	0.46	0.09
SF3B-3D	0.18	0.40	0.12	0.13 (0.19)	0.17 (0.46)	0.11 (0.10)	0.14	0.21	0.13	0.17	0.23	0.13	0.59	0.76	0.16

1. Peak acceleration calculated as spectral acceleration at 100 Hz
2. See Figure 6 for the global co-ordinate system
3. Not recorded

Table 6. Peak strain (μS) in internals for the 3D tests of the SFP-isolated configuration[1]

Test	Internal 1	Internal 2
SF1A-3D	208	74
SF1B-3D	172	117
SF2A-3D	179	97
SF2B-3D	226	107
SF3A-3D	137	80
SF3B-3D	213	95

1. For reference, the yield strain in internal 1 (internal 2) is approximately 4000 (1240) μS

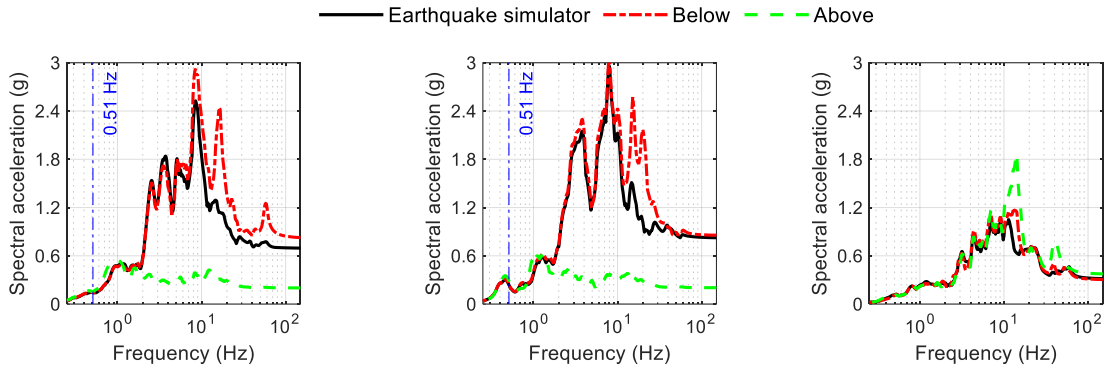

a) *x* direction b) *y* direction c) *z* direction

Figure 14. Acceleration response spectra directly above and below the isolation plane, test TF1B-3D, 5% damping

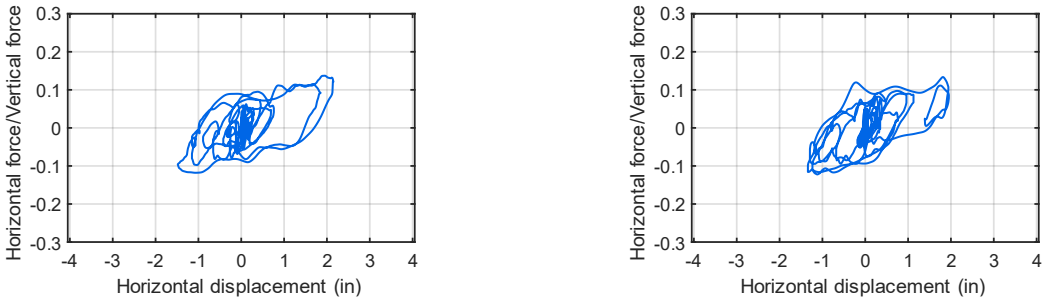

a) *x* direction b) *y* direction

Figure 15. Normalized force-displacement loops for the isolation system, test TF1B-3D

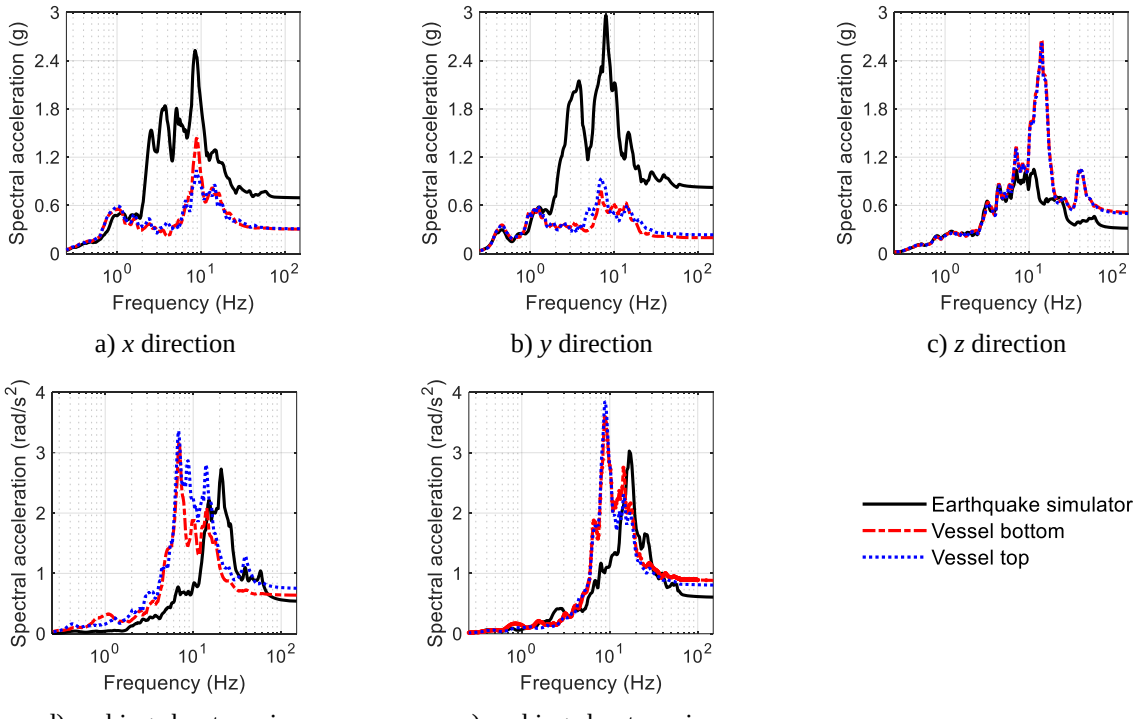

a) *x* direction b) *y* direction c) *z* direction

d) rocking about *x* axis e) rocking about *y* axis

Figure 16. Acceleration response spectra at the top and bottom of the vessel, test TF1B-3D, 5% damping

Table 7. Peak acceleration[1] (g) for the 3D tests of the TFP-isolated configuration, *x*, *y*, and *z* directions[2]

Test	Earthquake simulator			Directly above (below) the isolation plane			Vessel bottom			Vessel top			Internal 1 bottom		
	x	***y***	***z***	***x***	***y***	***z***	***x***	***y***	***z***	***x***	***y***	***z***	***x***	***y***	***z***
TF1A-3D	0.29	0.23	0.10	0.10 (0.30)	0.11 (0.27)	0.15 (0.12)	0.13	0.13	0.19	0.13	0.17	0.19	0.44	0.32	0.24
TF1B-3D	0.69	0.82	0.31	0.20 (0.81)	0.20 (0.85)	0.37 (0.31)	0.30	0.20	0.50	0.31	0.23	0.49	0.74	0.40	0.61
TF2A-3D	0.25	0.19	0.16	0.17 (0.32)	0.12 (0.32)	0.28 (0.21)	0.24	0.15	0.43	0.18	0.14	0.42	NR[3]	0.37	0.83
TF2B-3D	0.68	0.50	0.41	0.29 (1.07)	0.22 (0.87)	0.70 (0.58)	0.48	0.31	1.20	0.33	0.30	1.21	NR[3]	0.45	2.71
TF3A-3D	0.09	0.17	0.05	0.07 (0.11)	0.11 (0.18)	0.05 (0.05)	0.07	0.14	0.06	0.09	0.15	0.06	0.31	0.35	0.07
TF3B-3D	0.23	0.54	0.14	0.14 (0.24)	0.18 (0.56)	0.17 (0.14)	0.13	0.21	0.18	0.14	0.20	0.18	0.41	0.48	0.17

1. Peak acceleration calculated as spectral acceleration at 100 Hz
2. See Figure 6 for the global co-ordinate system
3. Not recorded

Table 8. Peak strain (μS) in internals for the 3D tests of the TFP-isolated configuration[1]

Test	Internal 1	Internal 2
TF1A-3D	98	67
TF1B-3D	94	110
TF2A-3D	95	90
TF2B-3D	99	146
TF3A-3D	94	72
TF3B-3D	141	119

1. For reference, the yield strain in internal 1 (internal 2) is approximately 4000 (1240) μS

horizontal response of the vessel was driven by its rocking at 11 Hz, which was amplified by the rocking of the earthquake-simulator platform due to simulator-specimen interaction. The frequencies of the vertical modes, driving the vessel's vertical response, were 17 Hz and 45 Hz. For moderate-to-high seismic inputs such as those in tests FB1B-3D and FB2B-3D, peak horizontal accelerations greater than 1 g were recorded at the top and the bottom of the vessel.

In the vertical direction, the amplification of spectral accelerations from the top of the load cells to the top and the bottom of the vessel was similar in the non-isolated and isolated configurations. Rocking of the isolated vessels was smaller than that in the non-isolated configuration given near-identical seismic inputs on the earthquake-simulator platform. The vertical flexibility of the bearings reduced the modal vertical and rocking frequencies from those in the non-isolated configuration.

Mid-height seismic isolation using SFP and TFP bearings generally enabled a significant reduction in the horizontal spectral accelerations above the isolation plane and at the top and the bottom of the vessel, with peak horizontal accelerations lower than those at the center of the earthquake-simulator platform in most cases. For moderate-to-high seismic inputs, and intensities greater than those in tests of the non-isolated configuration, the peak horizontal accelerations at the top and the bottom of the isolated vessel were less than 0.5 g. The efficacy of the isolation systems, measured in terms of the percentage reduction in the peak horizontal acceleration, was a function of the frequency content and the amplitude of the input motions. For design of isolated safety-class equipment in nuclear power plants, an isolation system could be tuned for the reactor- and site-specific seismic hazard (that is, the frequency content and the amplitude of shaking) to enable significant reductions in horizontal spectral accelerations: the isolation systems tested herein were not optimized across multiple ranges of frequency content and amplitude of seismic input.

The peak strains and the peak horizontal accelerations in the internals were smaller in the isolated configurations despite larger amplitude shaking being imposed. Peak horizontal accelerations greater than 1 g were observed at the bottom of internal 1 in the non-isolated configuration but were generally much smaller than 1 g in the isolated configurations for more intense seismic inputs.

The results from the earthquake-simulator tests of the vessel and its internals enable a qualitative comparison of the responses in the isolated and non-isolated configurations. Mid-height seismic isolation is beneficial and practical for tall, slender vessels. Although the focus herein was on safety-class equipment in advanced nuclear power plants, the results are applicable to tall, slender equipment regardless of industry sector. The outcomes are not specific to the spherical sliding bearings used in the experiments but are broadly applicable to mid-height, seismically isolated equipment.

Data availability statement

The data that support the findings of this study are available from the corresponding author upon reasonable request.

Acknowledgements

The information, data, or work presented herein was funded by the Advanced Research Projects Agency-Energy (ARPA-E), U.S. Department of Energy, under Award Number DE-AR0000978. The views and opinions of the authors expressed herein do not necessarily state or reflect those of the U.S. Government or any agency thereof. The authors thank the technical staff in the Structural Engineering and Earthquake Simulation Laboratory (SEESL) at the University at Buffalo for their assistance in fabricating and instrumenting the test article and executing the earthquake-simulator experiments. The authors also thank Earthquake Protection Systems for providing the SFP and TFP bearings at no cost.

7. References

[1] Tajirian, F. F. (1992). "Seismic analysis for the ALMR." *Proceedings: International Atomic Energy Agency (IAES) Specialists' Meeting on Seismic Isolation Technology*, San Jose, CA.

[2] Tajirian, F. F., and Patel, M. R. (1993). "Response of seismic isolated facilities: a parametric study of the ALMR." *Transactions: 12th International Conference on Structural Mechanics in Reactor Technology (SMiRT-12)*, Stuttgart, Germany.

[3] Aiken, I. D., Clark, P. W., and Kelly, J. M. (2002). "Experimental testing of reduced-scale seismic isolation bearings for the advanced liquid metal reactor." *Proceedings: IAEA-TECDOC-1288, Verification of analysis methods for predicting the behaviour of seismically isolated nuclear structures*, International Atomic Energy Agency (IAEA), Vienna, Austria.

[4] Huang, Y.-N., Whittaker, A. S., and Luco, N. (2008). "Performance assessment of conventional and base-isolated nuclear power plants for earthquake and blast loadings." Technical Report MCEER-08-0019, University at Buffalo, State University of New York, Buffalo, NY.

[5] Huang, Y.-N., Whittaker, A. S., Kennedy, R. P., and Mayes, R. L. (2009). "Assessment of base-isolated nuclear structures for design and beyond-design basis earthquake shaking." Technical Report MCEER-09-0008, University at Buffalo, State University of New York, Buffalo, NY.

[6] Kumar, M., Whittaker, A. S., and Constantinou, M. C. (2017). "Extreme earthquake response of nuclear power plants isolated using sliding bearings." *Nuclear Engineering and Design*, 316, 9-25.

[7] Kumar, M., Whittaker, A. S., Kennedy, R. P., Johnson, J. J., and Kammerer, A. (2017). "Seismic probabilistic risk assessment for seismically isolated safety-related nuclear facilities." *Nuclear Engineering and Design*, 313, 386-400.

[8] Yu, C.-C., Bolisetti, C., Coleman, J. L., Kosbab, B., and Whittaker, A. S. (2018). "Using seismic isolation to reduce risk and capital cost of safety-related nuclear structures." *Nuclear Engineering and Design*, 326, 268-284.

[9] Lal, K. M., Parsi, S. S., Kosbab, B. D., Ingersoll, E. D., Charkas, H., and Whittaker, A. S. (2022). "Towards standardized nuclear reactors: Seismic isolation and the cost impact of the earthquake load case." *Nuclear Engineering and Design*, 386, (https://doi.org/10.1016/j.nucengdes.2021.111487).

[10] Parsi, S. S., Lal, K. M., Kosbab, B. D., Ingersoll, E. D., Shirvan, K., and Whittaker, A. S. (2022). "Seismic isolation: A pathway to standardized advanced nuclear reactors." *Nuclear Engineering and Design*, 387, (https://doi.org/10.1016/j.nucengdes.2021.111445).

[11] Electric Power Research Institute (EPRI). (2013). "Seismic isolation of nuclear power plants." 3002000561, Palo Alto, CA.

[12] Kircher, C. A., Delfosse, G. C., Schoof, C. C., Khemici, O., and Shah, H. (1979). "Performance of a 230 kV ATB 7 power circuit breaker mounted on GAPEC seismic isolation." Report No. 40, The John A. Blume Earthquake Engineering Center, Stanford University, Stanford, CA.

[13] Kelly, J. M. (1983). "Use of base isolation and energy-absorbing restrainers for the seismic protection of a large power-plant component." Technical Report EPRI-NP-2918, Electric Power Research Institute, Palo Alto, CA.

[14] Buckle, I. G., and Mayes, R. L. (1990). "Seismic isolation: History, application, and performance - A world view." *Earthquake Spectra*, 6(2), 161-201.

[15] Kelly, T. E., and Mayes, R. L. (1989). "Seismic isolation of storage tanks." *Proceedings: Seismic engineering: Research and practice*, ASCE, 408-417.

[16] Tajirian, F. F. (1993). "Seismic isolation of critical components and tanks." *Proceedings: ATC-17-1, Seminar on Seismic Isolation, Passive Energy Dissipation, and Active Control*, San Francisco, California, 223-244.

[17] Zayas, V. A., and Low, S. S. (1995). "Application of seismic isolation to industrial tanks." *Proceedings: Joint American Society of Mechanical Engineers (ASME)/Japan Society of Mechanical Engineers (JSME) Conference on Pressure Vessels and Piping*, Honolulu, HI.

[18] Ersoy, S., Ala Saadeghvaziri, M., Liu, G.-Y., and Mau, S. T. (2001). "Analytical and experimental seismic studies of transformers isolated with friction pendulum system and design aspects." *Earthquake Spectra*, 17(4), 569-595.

[19] Murota, N., Feng, M. Q., and Liu, G.-Y. (2005). "Experimental and analytical studies of base isolation systems for seismic protection of power transformers." Technical Report MCEER-05-0008, University at Buffalo, State University of New York, Buffalo, NY.

[20] Oikonomou, K., Constantinou, M. C., Reinhorn, A. M., and Yenidogan, C. (2012). "Seismic isolation of electrical equipment - seismic table simulation." *Proceedings: 15th World Conference on Earthquake Engineering (15WCEE)*, Lisbon, Portugal.

[21] Oikonomou, K., Constantinou, M. C., Reinhorn, A. M., and Kemper Jr, L. (2016). "Seismic isolation of high voltage electrical power transformers." Technical Report MCEER-16-0006, University at Buffalo, State University of New York, Buffalo, NY.

[22] Cochran, R. (2015). "Seismic base isolation of a high voltage transformer." *Proceedings: Electrical Transmission and Substation Structures 2015*, Branson, Missouri, 413-425.

[23] Mir, F. U. H., Yu, C.-C., Whittaker, A. S., and Constantinou, M. C. (2022). "Physical and numerical simulations of seismic fluid-structure interaction in advanced nuclear reactor." Technical Report MCEER-22-0002, University at Buffalo, State University of New York, Buffalo, NY.

[24] Constantinou, M. C., Whittaker, A. S., Kalpakidis, Y., Fenz, D. M., and Warn, G. P. (2007). "Performance of seismic isolation hardware under service and seismic loading." Technical Report MCEER-07-0012, University at Buffalo, State University of New York, Buffalo, NY.

[25] Computers and Structures Incorporated (CSI). (2019). Computer Program SAP2000 (Version 20.2.0), Berkeley, CA.

[26] Lal, K. M., Whittaker, A. S., and Constantinou, M. C. (2022). "Earthquake-simulator test results: Mid-height isolated tall, slender vessel." Digital Appendix, (https://doi.org/10.6084/m9.figshare.21164842).

[27] Fenz, D. M., and Constantinou, M. C. (2008). "Mechanical behavior of multi-spherical sliding bearings." Technical Report MCEER-08-0007, University at Buffalo, State University of New York, Buffalo, NY.

[28] Fenz, D. M., and Constantinou, M. C. (2008). "Development, implementation and verification of dynamic analysis models for multi-spherical sliding bearings." Technical Report MCEER-08-0018, University at Buffalo, State University of New York, Buffalo, NY.